

Higher-order coupling effects in low energy heavy-ion fusion reactions

H. Esbensen and S. Landowne

Physics Division, Argonne National Laboratory, Argonne, Illinois 60439

(Received 8 January 1987)

Higher-order couplings to inelastic excitations of surface vibrations can strongly affect the enhancement of heavy-ion fusion cross sections at sub-barrier energies. Detailed second-order calculations are presented for reactions between different nickel isotopes. The agreement with measured fusion cross sections is considerably improved with respect to conventional coupled channels calculations based on linear couplings.

I. INTRODUCTION

It is now generally accepted that couplings to low-lying surface degrees of freedom—namely, rotations, vibrations, and valence particle transfer reactions—can cause pronounced enhancement effects on low energy heavy-ion fusion cross sections.¹ At present, quantitative fusion calculations which allow for such degrees of freedom have been successful for relatively light systems, such as O+Sm (Ref. 2) and Mg+S (Ref. 3). In most of these cases, the main dynamical effects have been due to rotational and first-order vibrational couplings. Studies of the doubly magic O+Pb reaction have shown large effects due to single-particle transfer couplings.^{4,5}

On the other hand, the low energy fusion cross sections for heavier mass systems, where the deviations from static model predictions are greatest, have not been well accounted for theoretically. For example, detailed coupled channels calculations for the Ni+Ni (Ref. 6) and Ar+Sn (Ref. 7) cases only produce about half of the effective shift in the Coulomb barrier. This has led to speculations that the neglected transfer reaction couplings, which are generally difficult to include explicitly in the calculations, should account for the discrepancies.^{6,8}

It is also appropriate to examine the assumptions which have been made concerning the surface vibrational degrees of freedom. For the most part, the calculations for heavier systems have treated the nuclear surface modes as independent harmonic oscillators which are linearly coupled to the relative motion. Moreover, the model spaces have either been truncated at the one-phonon level or have allowed for only a few higher order terms. It is reasonable to doubt that such types of restricted bases would be able to describe the evolution of two heavy, strongly coupled nuclei towards the fused state.^{9,10} In fact, a recent analysis of the Ti+Zr fusion reaction has been carried out using an extended vibrational basis.¹¹ It is clear that higher order coupling effects play an important role in these calculations (see, in particular, Table III of Ref. 11).

The purpose of the present paper is to study such effects in detail within a second-order vibrational model. In this way we can identify the main differences with respect to the previous first-order coupling schemes. We present detailed calculations for the Ni+Ni reaction which show that the second-order terms are as important as the linear

couplings in determining the low energy fusion cross section. As a result, the agreement with the data is significantly improved. We find, moreover, that the calculations appear to be converged.

The organization of this paper is as follows. The coupled channels formulation of the second-order model is given in the Sec. II. The adiabatic limit of the model is studied in Sec. III. Applications to the Ni+Ni reaction are presented in Sec. IV. The main conclusions of the work are summarized in Sec. V.

II. FORMALISM

The Hamiltonian for the problem we wish to consider is given as

$$H = H_{\text{rel}} + H_0 + V_{\text{cpl}}. \quad (1)$$

Here H_{rel} is the Hamiltonian for the relative motion in the elastic channel, consisting of the kinetic energy and the Coulomb and nuclear potentials,

$$H_{\text{rel}} = -\frac{\hbar^2 \nabla^2}{2\mu} + \frac{Z_1 Z_2 e^2}{r} + U(r). \quad (2)$$

The term H_0 represents the Hamiltonian for the intrinsic degrees of freedom. They will be modeled by a set of harmonic oscillators for the nuclear surface vibrations; namely

$$H_0 = \sum_{\alpha} \left[-\frac{\hbar^2}{2D_{\alpha}} \frac{\partial^2}{\partial s_{\alpha}^2} + \frac{1}{2} C_{\alpha} s_{\alpha}^2 - \frac{\hbar \omega_{\alpha}}{2} \right], \quad (3)$$

where $\omega_{\alpha} = \sqrt{C_{\alpha}/D_{\alpha}}$ denotes the vibrational frequency. Notice that the zero point energy has been subtracted here. This is done in order that the total energy at large distances is equal to the relative energy in the entrance channel, where the nuclei are in their ground states.

The Coulomb part of the coupling interaction between the relative and intrinsic motions is given to leading order in the surface amplitudes by

$$V_{\text{cpl}}^{(C)} = \frac{Z_1 Z_2 e^2}{r^2} \sum_{\alpha} \frac{3}{2\lambda_{\alpha} + 1} \left[\frac{R_c^{(\alpha)}}{r} \right]^{\lambda_{\alpha}^{-1}} s_{\alpha}, \quad (4)$$

where λ_{α} is the multipolarity of the vibration and R_c denotes the radius of the nuclear charge distribution. We

do not include second-order terms here. They are usually not important. Moreover, the simple adiabatic limit which is obtained below requires that the radial dependence of the second-order terms is the same for all modes. This is not true for the Coulomb field. For similar reasons of simplicity, we have followed the common prescription that the nuclear interaction depends on the separation of the vibrating surfaces; namely,

$$V_n = V_n(r - R_1 - R_2 - s), \quad (5)$$

where R_i is the average nuclear radius and s is the sum of the surface amplitudes,

$$s = \sum_{\alpha} s_{\alpha}. \quad (6)$$

The matrix elements of the nuclear interaction are the basic quantities to be specified. The expectation value in the ground state determines the nuclear ion-ion potential in the elastic channel,

$$U(r) = \langle 0 | V_n(r - R_1 - R_2 - s) | 0 \rangle. \quad (7)$$

It will be assumed that this function is known empirically. The transformation between the surface coordinates and the phonon creation and destruction operators is

$$\begin{aligned} s_{\alpha} &= \sigma_{\alpha}(a_{\alpha}^{\dagger} + a_{\alpha}), \\ d/ds_{\alpha} &= \frac{1}{2\sigma_{\alpha}}(a_{\alpha} - a_{\alpha}^{\dagger}), \end{aligned} \quad (8)$$

where σ_{α} is the zero-point amplitude defined by

$$\sigma_{\alpha}^2 = \langle 0 | s_{\alpha}^2 | 0 \rangle = \frac{\hbar\omega_{\alpha}}{2C_{\alpha}} \quad (9)$$

or, in terms of the beta value for the one phonon transition,

$$\sigma_{\alpha} = \beta_{\alpha} R_{\alpha} / \sqrt{4\pi}. \quad (10)$$

The matrix elements of V_n can then be worked out in terms of $U(r)$, its derivatives and powers of σ_{α} . Thus we need not specify V_n explicitly. For instance, the one-phonon excitation matrix element is the familiar expression

$$\begin{aligned} \langle 1 | V_n | 0 \rangle &= \langle 0 | [a_{\alpha}, V_n] | 0 \rangle \\ &= \sigma_{\alpha} \langle 0 | \partial V_n / \partial s_{\alpha} | 0 \rangle = -\sigma_{\alpha} (d/dr) U(r). \end{aligned} \quad (11)$$

The general matrix element is given in Appendix A. For the calculations we include couplings to second order and consider one- and two-phonon states. In the case of one mode there are six matrix elements, given in Eq. (A2). The extra couplings when additional modes are included, such as mutual excitation, are given in Eq. (A3).

In this work we neglect the fact that the excitation of each surface mode generally corresponds to a finite transfer of angular momentum. The calculations would become much more complicated if such effects were included. Fortunately, angular momentum transfer effects have little influence on total cross sections for heavy colliding systems at energies near and below the Coulomb

barrier. This has been shown by explicit numerical calculations⁶ and has been discussed in general terms in Ref. 12.

Notice in Eq. (A2) that the excited state diagonal terms are renormalized in second order. Since $U(r)$ and $U''(r)$ are negative in the barrier region, the nuclear attraction is increased in the excited states. This reflects the expectation that the nuclear surface is more diffuse in these states. As a result, the Coulomb barriers can be lowered in the inelastic channels.

The nuclear matrix elements given to second order in Appendix A and the first order Coulomb interaction of Eq. (4) are equivalent to introducing the coupling interaction

$$V_{\text{cpl}} = - \sum_{\alpha} F_{\alpha}(r) s_{\alpha} + \frac{U'''(r)}{2} s^2 - \frac{U''(r)}{2} \sum_{\alpha} \sigma_{\alpha}^2, \quad (12)$$

where

$$F_{\alpha}(r) = \frac{dU}{dr}(r) - \frac{Z_1 Z_2 e^2}{r^2} \frac{3}{2\lambda_{\alpha} + 1} \left[\frac{R_c^{(\alpha)}}{r} \right]^{\lambda_{\alpha} - 1}. \quad (13)$$

The last renormalization term in Eq. (12) has to be included so that the coupling interaction vanishes in the elastic channel.

The numerical calculations carried out below are based on solving a set of coupled radial wave equations of the form

$$(H_{\text{rel}} + n\hbar\omega - E)u_n(r) = - \sum_m \langle n | V_{\text{cpl}} | m \rangle u_m(r), \quad (14)$$

where E is the relative energy in the center of mass frame. The coupling term V_{cpl} is the difference between the total interaction and the potential in the elastic channel. It is given by Eq. (12) in the present model. The radial equations are solved under the usual scattering conditions at large distances which specify an incoming (Coulomb) wave in the elastic channel and outgoing waves in all channels. Ingoing wave boundary conditions are applied inside the Coulomb barrier, at the minimum of the effective potential. The ingoing flux at this point is equated to the flux which leads to fusion (see, for instance, Ref. 6 for additional details).

The above equations are written for one mode with frequency ω , but they can be immediately generalized to several modes. Let us mention that the number of coupled equations can be greatly reduced for symmetric reactions, since identical modes in the projectile and target can be represented by one mode. This can be seen by making an orthogonal transformation of the intrinsic Hamiltonian. For example, if there are two identical modes with amplitudes s_1 and s_2 , we may transform to new modes with amplitudes $x_1 = s_1 + s_2$ and $x_2 = s_1 - s_2$. Then x_1 is coupled to the relative motion but x_2 is not. The x_1 mode has the same frequency as the original modes, but the restoring force is only half as large. Thus the corresponding zero-point amplitude is larger by a factor of $\sqrt{2}$.

III. ADIABATIC LIMIT

The adiabatic description of heavy-ion fusion has been successful in reproducing coupled channels calculations at energies well below the barrier.⁷ It is instructive to study this limit for the model outlined above. A simple expression can be obtained for the adiabatic potential in the full phonon space. This case will be discussed here and will be contrasted with results obtained by numerically diagonalizing the truncated phonon space in Sec. IV.

In the adiabatic limit, the lowest energy state of the Hamiltonian for the intrinsic system in the presence of the coupling interaction

$$H_{\text{int}} = H_0 + V_{\text{cpl}} \quad (15)$$

enters effectively as a change in the ion-ion potential. It is easy to obtain this limit in the full phonon space when there is only one mode. In this case H_{int} can be written as

$$H_{\text{int}} = -\frac{\hbar^2}{2D_\alpha} \frac{\partial^2}{\partial s_\alpha^2} + \frac{(C_\alpha + U'')}{2} \left[s_\alpha - \frac{F}{C_\alpha + U''} \right]^2 - \frac{1}{2} \frac{F_\alpha^2}{(C_\alpha + U'')} - \frac{\hbar\omega_\alpha}{2} - \frac{U'}{2} \sigma_\alpha^2. \quad (16)$$

Therefore the adiabatic limit is

$$H_{\text{ad}} = \frac{\hbar\omega_\alpha}{2} (\sqrt{1 + U''/C_\alpha} - 1) - \frac{F_\alpha^2}{2(C_\alpha + U'')} - \frac{U''\sigma_\alpha^2}{2}. \quad (17)$$

The first term here is the change in the zero-point energy which appears because the quadratic coupling effectively modifies the restoring force of the surface mode. Allowing for changes in the zero-point energy in the adiabatic limit while tunneling is familiar from nuclear fission studies.¹³ The adiabatic limit for tunneling with linear coupling to an oscillator ($U''=0$) was studied in Ref. 14. An approximate expression for the case of purely quadratic coupling ($F_\alpha=0$) was given in Ref. 15 [Eq. (6.31) of Ref. 15 corresponds to expanding the change in the zero-point energy to third order in U''/C_α].

Since U'' is negative in the present case, the frequency is effectively reduced, which in turn tends to invalidate the adiabatic condition. It is also seen that H_{ad} diverges when $U''\sigma_\alpha^2 = -\hbar\omega_\alpha/2$. This unphysical behavior occurs because the adiabatic limit is obtained for an infinite phonon number space, whereas the interaction has only been expanded to second order in the vibrational amplitudes. The adiabatic potential obtained numerically in the truncated space of one- and two-phonon excitations is well behaved.

The adiabatic limit for a collection of independent modes would just be given by a sum of terms as in Eq. (17). This is not true for the present model since there are quadratic couplings between the modes. The general expression is derived in Appendix B. It is analytic up to a diagonalization which determines the new zero-point energies $\hbar\epsilon_\alpha/2$. The result is

$$H_{\text{ad}} = \sum_\alpha \frac{1}{2} (\hbar\epsilon_\alpha - \hbar\omega_\alpha - U''\sigma_\alpha^2) + V_{\text{ad}}, \quad (18)$$

where the interaction part is [cf. Eqs. (B1)–(B3) and (B7)]

$$V_{\text{ad}} = - \sum_\alpha \frac{F_\alpha^2}{2C_\alpha} + \frac{U''}{2} \frac{\left[\sum_\alpha F_\alpha/C_\alpha \right]^2}{(1 + U''/C)} \quad (19)$$

and

$$1/C = \sum_\alpha \frac{1}{C_\alpha}. \quad (20)$$

If we take a common value F for F_α , the expression for V_{ad} reduces to

$$V_{\text{ad}} \simeq - \frac{F^2}{2(C + U'')} \quad (21)$$

which has the same form as for a single mode. It is interesting to compare V_{ad} to the corresponding result obtained when the coupling between the modes is neglected, which is

$$V_{\text{ad}}^{(i)} = - \sum_\alpha \frac{F_\alpha^2}{2(C_\alpha + U'')}. \quad (22)$$

Taking again a common value for F_α and letting $C_\alpha \simeq NC$, where N is the number of modes, we have

$$V_{\text{ad}}^{(i)} \simeq - \frac{F^2}{2(C + U''/N)}. \quad (23)$$

The comparison of this result to Eq. (21) indicates that quadratic couplings between modes can be quite effective in increasing the strength of V_{ad} .

Let us finally note that in the linear coupling limit ($U''=0$) the modes are independent and H_{ad} becomes simply

$$H_{\text{ad}}^{(\text{lin})} = - \sum_\alpha \frac{(F_\alpha \sigma_\alpha)^2}{\hbar\omega_\alpha} = - \sum_\alpha \frac{|\langle \alpha | V_{\text{cpl}} | 0 \rangle|^2}{\hbar\omega_\alpha}. \quad (24)$$

This is just the usual expression for the adiabatic potential. It may be compared to the lowest eigenvalue of H_{int} for the one-phonon product space, which is¹⁶

$$\lambda_{\text{min}} = \sum_\alpha \frac{\hbar\omega_\alpha - [(\hbar\omega_\alpha)^2 + 4(F_\alpha \sigma_\alpha)^2]^{1/2}}{2}. \quad (25)$$

Inspection shows that λ_{min} is less negative than $H_{\text{ad}}^{(\text{lin})}$ and becomes equal to it when the ratios $(2F_\alpha \sigma_\alpha / \hbar\omega_\alpha)^2$ are much less than one.

IV. APPLICATIONS

We will consider the case of $^{58}\text{Ni} + ^{58}\text{Ni}$ in some detail since there have been several previous studies of this system. To illustrate the essential points, we take the 2^+ and 3^- levels as our basic one-phonon states. The corresponding values for σ_λ are given in Table I, together with the potential parameters we have used. We note that the σ_λ values are listed multiplied by a factor of $\sqrt{2}$ because the reaction is symmetric. Our coupling matrix consists of just those elements summarized in Appendix A, utilizing the scaled values of σ_λ . This automatically takes mutual

TABLE I. One-phonon excitation energies $\hbar\omega_\lambda$, β_λ values, and the associated standard deviation of surface amplitudes $\sqrt{2}\sigma_\lambda$ used in the coupled channels calculations for reactions between different nickel isotopes. Average values have been used for the reaction $^{58}\text{Ni} + ^{64}\text{Ni}$.

Reaction	λ	$\hbar\omega_\lambda$ (MeV)	β_λ	$\sqrt{2}\sigma_\lambda$ (fm)	ΔR (fm) ^a
$^{58}\text{Ni} + ^{58}\text{Ni}$	2 ⁺	1.45	0.187	0.337	0.00 ^b
	3 ⁻	4.47	0.20	0.368	
$^{64}\text{Ni} + ^{64}\text{Ni}$	2 ⁺	1.34	0.19	0.355	0.20
	3 ⁻	3.56	0.18	0.336	
$^{58}\text{Ni} + ^{64}\text{Ni}$	2 ⁺	1.4		0.346	0.14
	3 ⁻	4.0		0.352	

^aPotential from Ref. 17 [Sec. III 1, Eqs. (40)–(43)]:

$$U(r) = -31.67 \frac{R_1 R_2}{R_1 + R_2} \times \left[1 + \exp \left(\frac{r - R_1 - R_2 - \Delta R}{a} \right) \right]^{-1} \text{ (MeV)},$$

$$R_i = 1.233 A_i^{1/3} - 0.98 A_i^{-1/3} \text{ (fm)}, \quad a = 0.63 \text{ fm}.$$

^b $\Delta R = 0.08$ fm is used in Fig. 5 for $^{58}\text{Ni} + ^{58}\text{Ni}$.

projectile-target excitations of identical modes into account.

The parameters for the nuclear ion-ion potential in Table I are based on the empirical potential of Ref. 17. We have adjusted the nuclear radius in order that the fusion calculations agree with the measured cross section at higher energies.¹⁸ The results of the calculations are shown in Fig. 1. The lowest curve is obtained without coupling. The middle solid curve results when only one-phonon states with linear couplings are included. This produces a shift of about 2 MeV in the low energy cross section, which is in agreement with the effects observed in

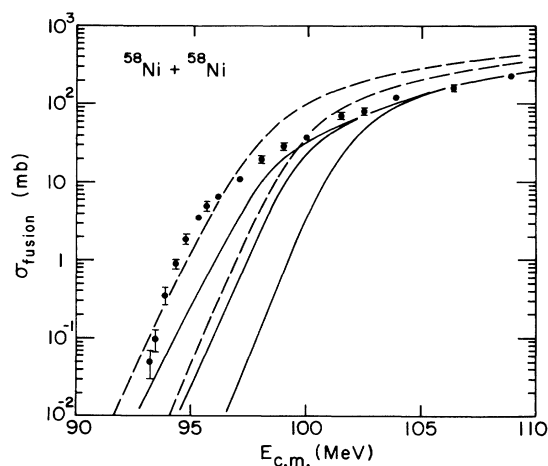


FIG. 1. Calculated fusion cross sections for $^{58}\text{Ni} + ^{58}\text{Ni}$ compared to the data of Ref. 18. The solid curves show, in increasing order, the no coupling limit, linear coupling only, and linear-plus-quadratic couplings for the 2⁺ and 3⁻ vibrational modes. The dashed curves show the corresponding first- and second-order adiabatic limits.

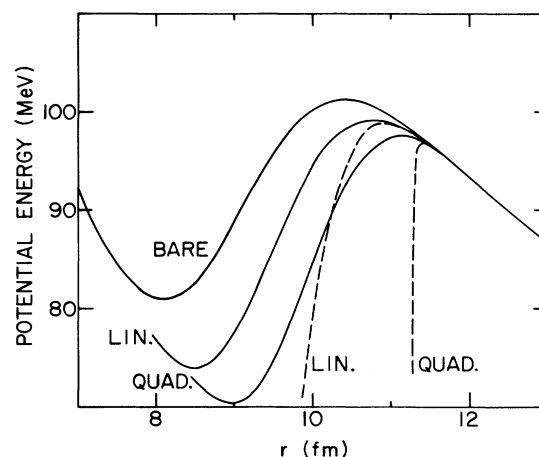


FIG. 2. Adiabatic potentials for $^{58}\text{Ni} + ^{58}\text{Ni}$ corresponding to the truncated linear and linear-plus-quadratic coupling schemes in comparison with the bare potential. The dashed curves are calculated with the full phonon space expression of Eq. (19).

other similar calculations.^{3,6} The new result is shown by the uppermost solid curve which also allows for two-phonon states and quadratic coupling terms. There is a dramatic effect on the low energy cross sections. They are shifted by an additional 1.8 MeV. We find that about half of this shift results when the off-diagonal quadratic couplings are set to zero but the potential renormalization terms are retained. Clearly, such large effects are required to make a significant improvement between theory and experiment.

The dashed curves shown in Fig. 1 result from one-dimensional barrier penetration calculations using the adiabatic potentials obtained by diagonalizing the matrices for the coupled intrinsic system.⁷ They roughly account for the full coupled channels calculations at low energies. The deviation increases in second order. In any case, the relative shift between the first and second-order calculations is tracked by the adiabatic barriers.

The corresponding adiabatic potentials are plotted in Fig. 2. This figure also conveys the strong influence of the quadratic couplings. The dashed curves in Fig. 2 are the potentials calculated using the analytic expression of Eq. (19). The additional contribution to Eq. (18) is small. Clearly, using these potentials in one-dimensional barrier penetration calculations would give even poorer comparisons with the coupled channels results in the truncated spaces. In fact, the sharp drop of the potential for quadratic coupling reflects the unphysical divergence noted in connection with Eq. (17). Nevertheless, the barrier heights obtained from the formulae are in qualitative agreement with those obtained numerically. In general, the correspondence should improve as the adiabatic limit is approached.

We will now examine the convergence of the calculations. For this purpose, we will restrict the model to include only the 2⁺ mode. We also perform the calculations only for the *s*-wave barrier penetration probability. The set of results in Fig. 3 compare linear and quadratic coupling calculations for zero excitation frequencies. In

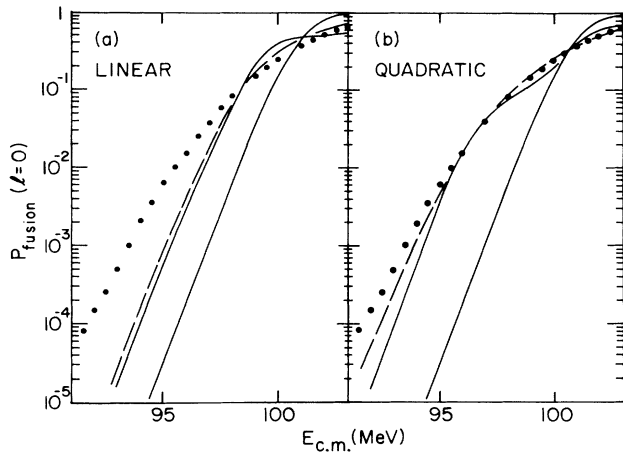


FIG. 3. Transmission probabilities for the $^{58}\text{Ni} + ^{58}\text{Ni}$ s -wave barrier allowing for the coupling to the 2^+ vibration and setting $\hbar\omega = 0$. In both figures the lower solid curve is the no-coupling limit, whereas the dotted curve incorporates essentially all orders for the nuclear coupling. Panel (a) compares the result for linear coupling truncated at the one-phonon level (upper solid curve) to linear couplings with an infinite phonon number (dashed curve). Panel (b) is the corresponding comparison for the linear-plus-quadratic couplings. The upper solid curve is obtained by truncating at the two-phonon level.

each case the one-dimensional result is shown for comparison. It gives the lowest transmission probability at energies below the barrier.

Consider first Fig. 3(a), which corresponds to linear coupling with zero frequency. In this case one can include the full, infinite phonon number space by using the "zero-point motion" (ZPM) limit.¹⁹ The ZPM result is

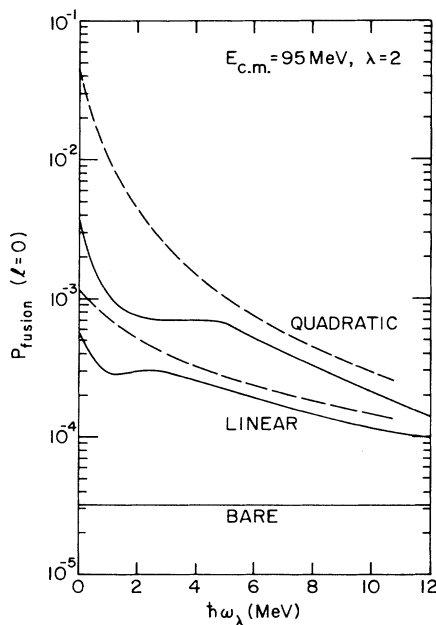


FIG. 4. Transmission probabilities as a function of one-phonon excitation energy in the linear and linear-plus-quadratic coupling schemes. The dashed curves are the corresponding adiabatic limits.

shown by the dashed curve in Fig. 3(a). It is close to the corresponding coupled channels calculation using only one phonon. This demonstrates that there is little to be gained by simply increasing the number of phonons with linear coupling.

On the other hand, allowing for two phonons with additional quadratic coupling produces the large effects shown in Fig. 3(b). The dashed curve here is the corresponding infinite phonon number limit. This indicates that two phonons are sufficient.

Finally, we consider the exact result in the zero frequency limit. This is obtained using the complete s -dependent interaction. The dotted curves in Fig. 3 show the result of a converged calculation which uses 20 phonons with all compatible matrix elements computed according to Eq. (A1). It is seen in Fig. 3(a) that the linear expansion gives a poor representation of the exact result at low energies. On the other hand, the quadratic approximation in Fig. 3(b) gives relatively good agreement. This result can be understood qualitatively by noting that in the barrier region the Eq. (A1) corresponds approximately to an expansion in the parameter σ_α/a , where a is the nuclear diffusivity. This parameter is about 0.5 for the present case.

Since the zero frequency calculations converge rapidly with the number of phonons and are well approximated using quadratic couplings, one should expect an even more rapid convergence for finite excitation frequencies. Difficulties can arise in such multiphonon calculations, however, due to channels which have decaying wave functions.¹⁰

A study of the finite frequency effect in the first and second-order coupling schemes is shown in Fig. 4. Here we show the s -wave penetration probability well below the barrier as a function of the 2^+ excitation energy. The dashed curves are the corresponding adiabatic limits. There is a significant difference between the linear and quadratic coupling results up to rather large excitation energies.

The implication that high lying states must be included is, however, not so clear because it is not straightforward to generalize the results from one mode to several combined modes. For example, we have found that adding the giant quadrupole mode, which exhausts 70% of the energy weighted sum rule ($\hbar\omega_\alpha = 15$ MeV, $\sigma_\alpha = 0.34$ fm), to the calculations does not significantly change the cross sections shown in Fig. 1.

We have also applied our model to the reactions between different nickel isotopes. The results are displayed in Fig. 5 together with the measured fusion cross sections.¹⁸ The calculations are based on one- and two-phonon excitations of the low-lying 2^+ and 3^- states given in Table I, including all first- and second-order couplings. We have used a slightly larger potential radius for the $^{58}\text{Ni} + ^{58}\text{Ni}$ reaction ($\Delta R = 0.08$ fm) than was applied in the preceding calculations in order to get a better overall agreement with the data. The value adopted for the $^{64}\text{Ni} + ^{64}\text{Ni}$ reaction was even larger ($\Delta R = 0.20$ fm). This choice is consistent with the isotope dependence of the neutron rms radius for the nickel isotopes obtained in recent shell model calculations.²⁰ We note that the overall

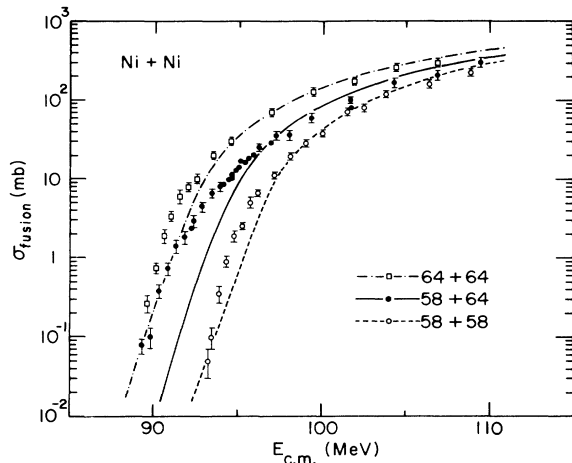


FIG. 5. Comparison of second-order vibrational calculations with the fusion data of Ref. 18 for the $^{58}\text{Ni}+^{58}\text{Ni}$, $^{58}\text{Ni}+^{64}\text{Ni}$, and $^{64}\text{Ni}+^{64}\text{Ni}$ reactions. The parameters are given in Table I.

agreement with the data has the same quality for these two reactions. The calculations are on the high side of the data at the highest beam energies. At the lower energies, the deviations from the data are less than 1 MeV. This is a considerable improvement compared to previous calculations based on linear nuclear couplings,⁶ where the deviations were about 3 MeV.

The discrepancy for the $^{58}\text{Ni}+^{64}\text{Ni}$ reaction is more dramatic at the lower energies, where the deviations are of the order of 2 MeV. Other measurements have shown that the one- and two-neutron transfer cross sections are much larger for this reaction than for the $^{58}\text{Ni}+^{58}\text{Ni}$ and the $^{64}\text{Ni}+^{64}\text{Ni}$ reactions.^{8,21} Since the surface modes for the two nickel isotopes are quite similar, it is natural to suspect that coupling to transfer channels may resolve the remaining discrepancy. Indeed, a previous analysis obtained reasonable results for $^{58}\text{Ni}+^{64}\text{Ni}$ by including two-particle transfer channels with positive Q values within a macroscopic model.²² We have made similar calculations treating the two-neutron transfer coupling effectively as a monopole vibration with positive Q value. We included it to second order on equal footing with the 2^+ and 3^- states, and adjusted the strength to fit the observed transfer cross sections.⁸ The effect on fusion was to bring the calculations much closer to the data below the barrier. We intend to make a more systematic study of the transfer reactions in a future communication.

Finally, it is of interest to know when it is important to include higher-order coupling effects. In general, the interactions in the barrier region become weaker for lighter mass systems or for more asymmetric reactions. Also the coupling effects are reduced as the excitation energy increases. We have, in particular, considered the case of $^{40}\text{Ca}+^{40}\text{Ca}$, where there is a collective 3^- state. Here we find that the second-order couplings shifted the calculations below the barrier by an additional amount of 0.4 MeV, compared to a 1 MeV shift generated by the purely linear coupling. Such a change is within the uncertainty of the underlying potential used to fit the data (see Ref.

23). On the other hand, the case of $^{74}\text{Ge}+^{74}\text{Ge}$ has a strong 2^+ state at 0.596 MeV ($\sigma \sim 0.4$ fm) and a 3^- state at 2.537 MeV. Here we find a first-order shift of about 2.5 MeV. Including the second-order couplings increases this to about 5 MeV. We estimate, however, that a shift of more than 10 MeV is required to fit the data of Ref. 24. Moreover, our calculations for this reaction have not converged in second order.

V. CONCLUSIONS

In this work we have seen that second-order couplings within a surface vibrational model can produce significant additional enhancements of low energy heavy-ion fusion cross sections. For the case of Ni+Ni reactions, these effects are as large as those that have previously been calculated in the conventional first-order model. Similar results are expected to occur for many combinations of medium heavy nuclei. For lighter or more asymmetric reactions, where the nuclear couplings are weaker, the second-order couplings are less important. Our calculations for the heavier system of Ge+Ge indicate that second-order calculations are not sufficient.

The additional physical features which occur in second order are the direct excitation of two-phonon states, the renormalization of excited state potentials, and the interaction between different modes. One would expect that such processes are generally present and not just limited to the particular vibrational model used here. Eventually, more fundamental calculations should be carried out. It may be noted that one would have to go beyond the random phase approximation in order to calculate potential renormalizations microscopically. It is intriguing to consider that the low energy fusion cross sections of heavy nuclei may provide a means for studying such nuclear structure problems.

We have found that the adiabatic limit of the model provides a helpful insight into the mechanisms affecting the low energy coupled channels calculations. However, the adiabatic limit becomes less applicable when the second-order processes are included.

Finally, we have been able to obtain an improved agreement with the low energy fusion data for $^{58}\text{Ni}+^{58}\text{Ni}$ and $^{64}\text{Ni}+^{64}\text{Ni}$ using the second-order surface vibrational model. Discrepancies remain, particularly for the $^{58}\text{Ni}+^{64}\text{Ni}$ reaction, which presumably are due to the neglected transfer reaction channels.

This work was supported by the U. S. Department of Energy under Contract No. W-31-109-ENG-38.

APPENDIX A: NUCLEAR COUPLINGS

The matrix elements between multiphonon states of the nuclear interaction discussed in Sec. II can be expressed in terms of derivatives of the ion-ion potential in the elastic channels. The general expression can be derived similarly to Eq. (11) using commutators. For n - and m -phonon states of the same mode one finds that for $m \leq n$

$$\langle n | V_n | m \rangle = \sum_{p=0}^m \frac{\sqrt{m!n!}}{(m-p)!p!(n-m+p)!} \times \left[-\sigma_\alpha \frac{\partial}{\partial r} \right]^{n-m+2p} U(r). \quad (\text{A1})$$

There are six different matrix elements to consider when we truncate at the two-phonon level. If we include all terms in (A1) up to second order we obtain the following expressions:

$$\begin{aligned} \langle 0 | V_n | 0 \rangle &= U(r), \\ \langle 1 | V_n | 1 \rangle &= U(r) + \sigma_\alpha^2 U''(r), \\ \langle 2 | V_n | 2 \rangle &= U(r) + 2\sigma_\alpha^2 U''(r), \\ \langle 1 | V_n | 0 \rangle &= -\sigma_\alpha U'(r), \\ \langle 2 | V_n | 1 \rangle &= -\sqrt{2}\sigma_\alpha U'(r), \\ \langle 2 | V_n | 0 \rangle &= 1/\sqrt{2}\sigma_\alpha^2 U''(r). \end{aligned} \quad (\text{A2})$$

When two (or more) different modes are present we also have to consider the mutual excitation state $|11\rangle$. In this case there are the following first- and second-order couplings between the modes:

$$\begin{aligned} \langle 11 | V_n | 10 \rangle &= -\sigma_\alpha U'(r), \\ \langle 11 | V_n | 01 \rangle &= -\sigma_\beta U'(r), \\ \langle 11 | V_n | 00 \rangle &= \langle 10 | V_n | 01 \rangle = \sigma_\alpha \sigma_\beta U''(r), \\ \langle 11 | V_n | 11 \rangle &= U(r) + (\sigma_\alpha^2 + \sigma_\beta^2) U''(r), \\ \langle 20 | V_n | 11 \rangle &= \langle 02 | V_n | 11 \rangle = \sqrt{2}\sigma_\alpha \sigma_\beta U''(r), \end{aligned} \quad (\text{A3})$$

APPENDIX B: ADIABATIC POTENTIAL

In the general case we first minimize the interaction part of $H_{\text{int}} = H_0 + V_{\text{cpl}}$. This leads to the condition

$$C_\alpha s_\alpha^{\text{ad}} + U'' s_{\text{ad}} = F_\alpha, \quad (\text{B1})$$

where

$$s_{\text{ad}} = \sum_\alpha s_\alpha^{\text{ad}} \quad (\text{B2})$$

is the total adiabatic surface distortion. Isolating s_α^{ad} and summing leads to the result

$$s_{\text{ad}} = \frac{\sum_\alpha F_\alpha / C_\alpha}{1 + U'' / C}, \quad \frac{1}{C} = \sum_\alpha \frac{1}{C_\alpha}. \quad (\text{B3})$$

The individual adiabatic distortions are now completely specified. We can rewrite H_{int} as

$$\begin{aligned} H_{\text{int}} = \sum_\alpha \left[-\frac{\hbar^2}{2D_\alpha} \frac{\partial^2}{\partial s_\alpha^2} + \frac{1}{2} \sum_\beta C_{\alpha\beta} (s_\alpha - s_\alpha^{\text{ad}})(s_\beta - s_\beta^{\text{ad}}) \right. \\ \left. - \frac{F_\alpha}{2} s_\alpha^{\text{ad}} - \frac{\hbar\omega_\alpha}{2} - \frac{U''}{2} \sigma_\alpha^2 \right], \end{aligned} \quad (\text{B4})$$

where

$$C_{\alpha\beta} = C_\alpha \delta_{\alpha,\beta} + U''. \quad (\text{B5})$$

Finally, we must determine the zero-point energy associated with the oscillations about the adiabatic coordinates. The complication that the mass parameters are not the same for the different modes can be overcome by scaling the coordinate s_α by $\sqrt{D_\alpha}$. This leads to the following matrix for the square of the frequencies:

$$\omega_\alpha^2 = C_\alpha / D_\alpha \delta_{\alpha,\beta} + U'' / \sqrt{D_\alpha D_\beta}. \quad (\text{B6})$$

Let ϵ_α^2 be the eigenvalues obtained by diagonalizing this matrix. Then $\hbar\epsilon_\alpha/2$ determines the new zero-point energies. The final result for the adiabatic limit is thus

$$H_{\text{ad}} = \sum_\alpha \frac{1}{2} (\hbar\epsilon_\alpha - \hbar\omega_\alpha - U'' \sigma_\alpha^2) - \frac{1}{2} \sum_\alpha F_\alpha s_\alpha^{\text{ad}}. \quad (\text{B7})$$

¹For a review, see M. Beckerman, *Phys. Rep.* **129**, 145 (1985).

²R. G. Stokstad and E. E. Gross, *Phys. Rev. C* **23**, 281 (1981).

³M. J. Rhoades-Brown and P. Braun-Munzinger, *Phys. Lett.* **136B**, 19 (1984).

⁴I. J. Thompson, M. A. Nagarajan, J. S. Lilley, and B. R. Fulton, *Phys. Lett.* **157B**, 250 (1985).

⁵S. C. Pieper, M. J. Rhoades-Brown, and S. Landowne, *Phys. Lett.* **162B**, 43 (1985).

⁶S. Landowne and S. C. Pieper, *Phys. Rev. C* **29**, 1352 (1984).

⁷O. Tanimura, J. Makowka, and U. Mosel, *Phys. Lett.* **163B**, 317 (1985).

⁸K. E. Rehm, F. L. H. Wolfs, A. M. van den Berg, and W. Henning, *Phys. Rev. Lett.* **55**, 280 (1985).

⁹H. J. Krappe, K. Moehring, M. C. Nemes, and H. Rosner, *Z. Phys. A* **314**, 23 (1983).

¹⁰H. Esbensen, J.-Q. Wu, and G. F. Bertsch, *Nucl. Phys.* **A411**, 275 (1983).

¹¹J.-Q. Wu and G. F. Bertsch, *Nucl. Phys.* **A457**, 894 (1986).

¹²C. H. Dasso and S. Landowne, *Z. Phys. A* **322**, 175 (1985).

¹³J. Maruhn and W. Greiner, *Phys. Lett.* **44B**, 9 (1973).

¹⁴D. M. Brink, M. C. Nemes, and D. Vautherin, *Ann. Phys.*

(N.Y.) **147**, 171 (1983).

¹⁵A. B. Balantekin and N. Takigawa, *Ann. Phys. (N.Y.)* **160**, 441 (1985).

¹⁶C. H. Dasso, S. Landowne, and A. Winther, *Nucl. Phys.* **A407**, 221 (1983).

¹⁷R. A. Broglia and A. Winther, *Heavy Ion Reactions, Lecture Notes* (Benjamin, New York, 1981), Vol. 1.

¹⁸M. Beckerman, M. Salomaa, A. Sperduto, H. Enge, J. Ball, A. DiRienzo, S. Gazes, Yan Chen, J. D. Molitoris, and Mao Nai-feng, *Phys. Rev. Lett.* **45**, 1472 (1980).

¹⁹H. Esbensen, *Nucl. Phys.* **A352**, 147 (1981).

²⁰B. A. Brown (private communication).

²¹J. Wiggins, R. Brooks, M. Beckerman, S. B. Gazes, L. Grodzins, A. P. Smith, S. G. Steadman, Y. Xiao, and F. Videbaek, *Phys. Rev. C* **31**, 1315 (1985).

²²R. A. Broglia, C. H. Dasso, and S. Landowne, *Phys. Rev. C* **32**, 1426 (1985).

²³S. Landowne, C. H. Dasso, R. A. Broglia, and G. Pollarolo, *Phys. Rev. C* **31**, 1047 (1985).

²⁴M. Beckerman, M. K. Salomaa, J. Wiggins, and R. Rohe, *Phys. Rev. C* **28**, 1963 (1983).